Supporting Information

Portable and non-invasive fluorescent thin films from photocatalytically active carbon dots for selective and trace level detection of picric acid

Nirmiti Mate [a], Divya Khandelwal [a], Kallayi Nabeela [a], and Shaikh M. Mobin *[, abc.]

[a] Department of Chemistry, Indian Institute of Technology Indore, Simrol, Khandwa Road, Indore 453552, India.

[b] Centre for Electric Vehicle and Intelligent Transport Systems, Indian Institute of Technology Indore, Simrol, Khandwa Road, 433552, India

[c] Centre for Advanced Electronics (CAE), Indian Institute of Technology, Indore, Simrol, Madhya Pradesh, India.

*Corresponding author

Email: xray@iiti.ac.in (Shaikh M. Mobin)

Tel.: +91-731-2438752

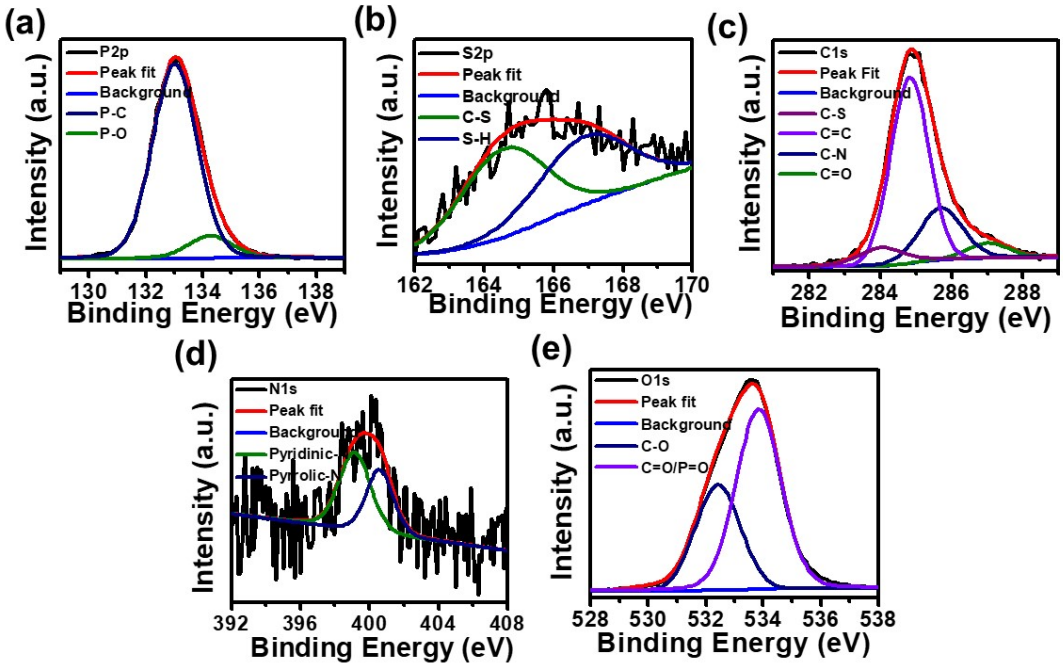

Figure S1. Deconvoluted high resolution XPS spectra of TF-CDs: (a) P2p (b) S2p (c) C1s (d) N1s and (e) O1s.

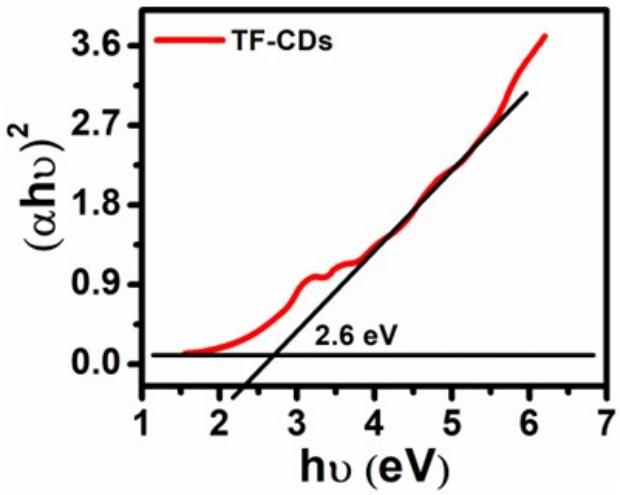

Figure S2. Plot of $(\alpha hv)^2$ versus photo energy (hv) for TF-CDs.

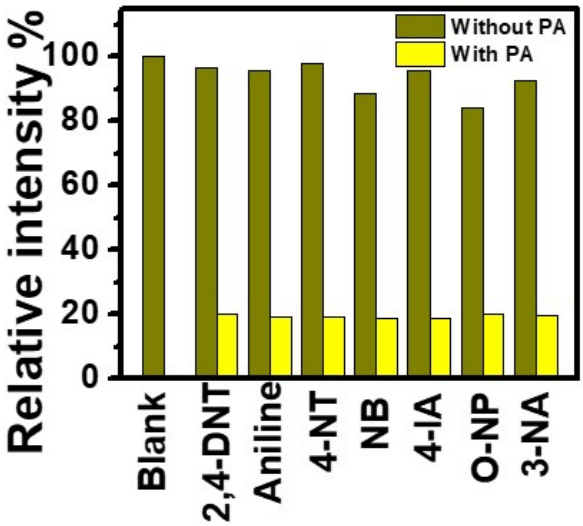

Figure S3. Competitive selectivity in the sensing response of TF-CDs in presence nitro aromatic compound ($c = 1.0 \times 10^{-2}$ M).

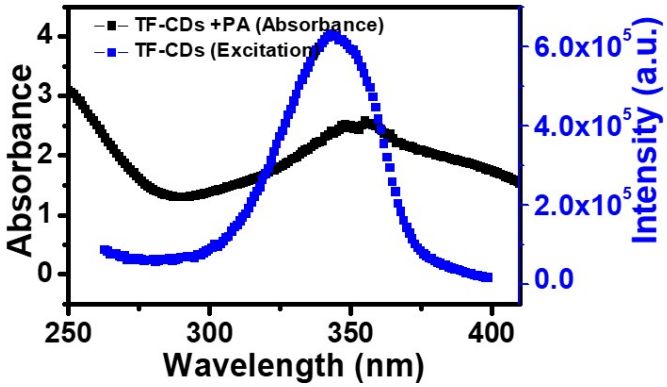

Figure S4. UV-vis absorption spectra of TF-CDs with addition of PA (black line) and maximum fluorescence excitation of TF-CDs (blue line) showing spectral overlapp.

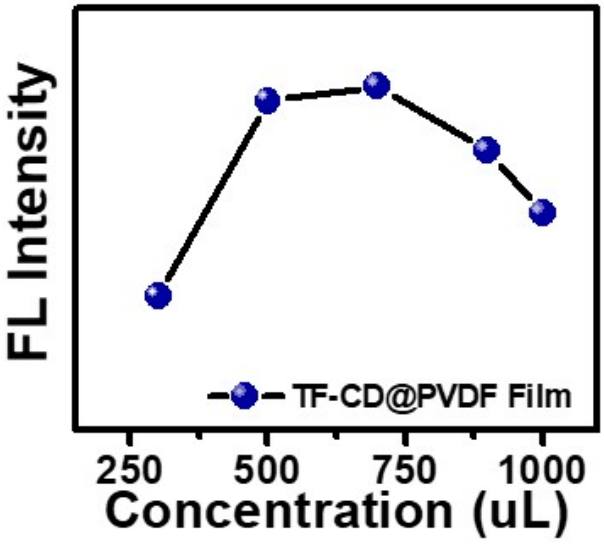

Figure S5. Effect on FL property of TF-CD@PVDF by varying the concentration of TF-CDs.

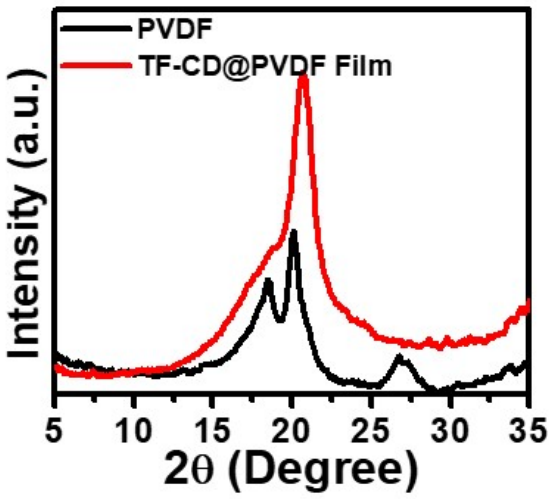

Figure S6. PXRD of PVDF and TF-CD@PVDF

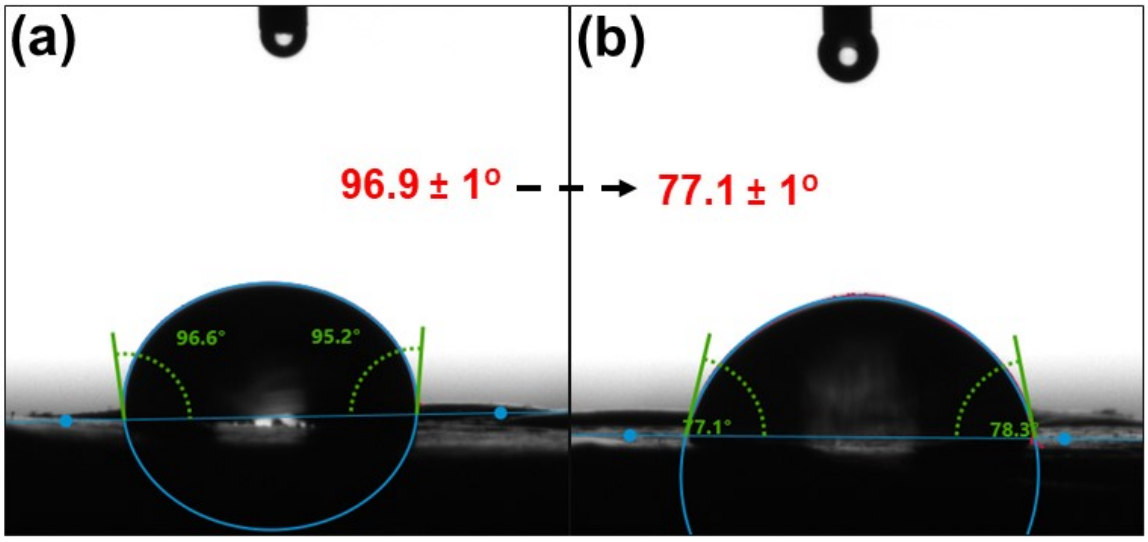

Figure S7. Sessile drop contact angle (θ) measurements of the (a) PVDF membrane (b) TF-CD@PVDF.

1. The stability of TF-CDs@PVDF film

The stability of TF-CDs@PVDF film was determined at various pH, by varying the concentration of NaCl and at various temperature. The TF-CDs@PVDF stability as depicted in Figure S8(a-c). The film is relatively stable in pH range of 3-11 as indicated in Figure S8a. Under adverse NaCl concentration as shown in Figure S8b the film is stable and retain the FL up to 79%. Similarly, FL was stable at different temperatures up to 96% when kept at −21 °C, 3 °C, 20 °C, 37 °C and 100 °C as indicate in Figure S8c.

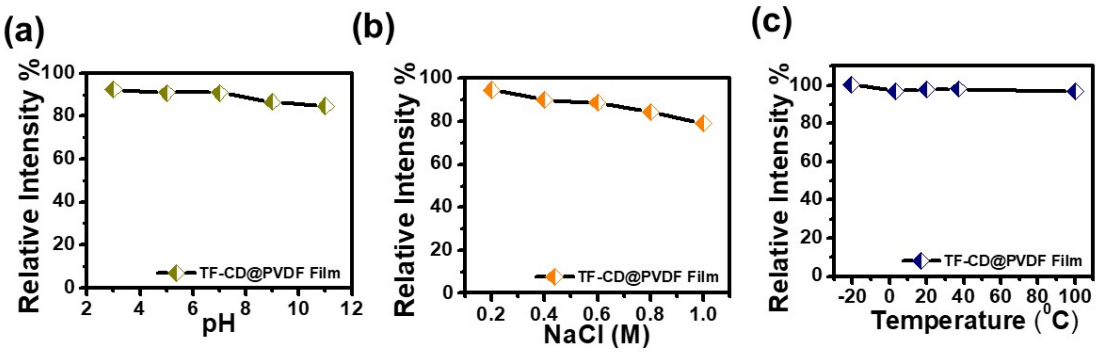

Figure S8. The stability of TF-CD@PVDF film under different: (a) pH (b) NaCl concentrations (c) temperature.

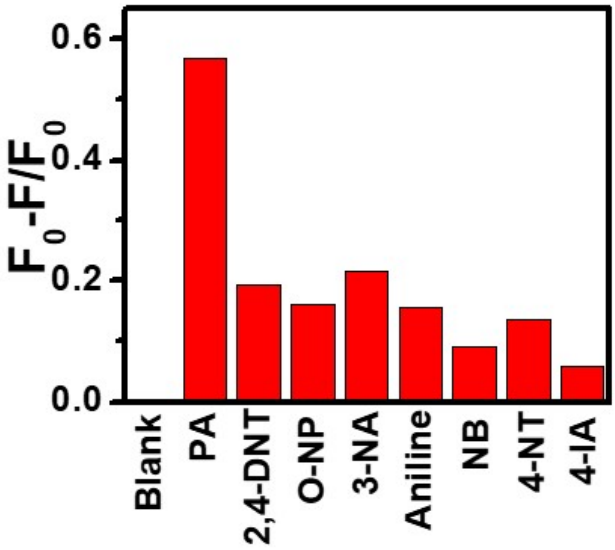

Figure S9. The selectivity of TF-CD@PVDF film towards various NACs.

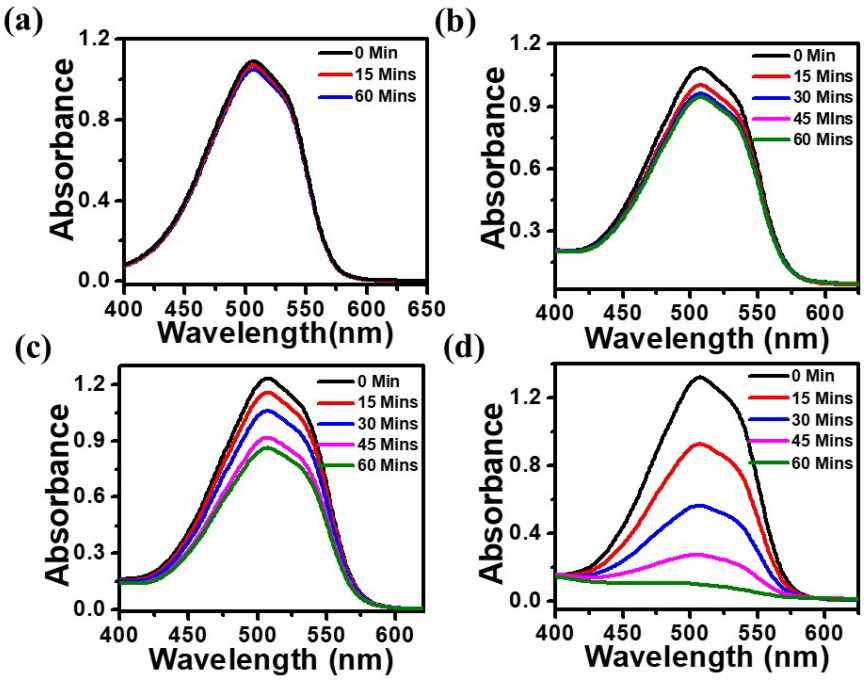

Figure S10. (a) Degradation of MO without catalyst in sunlight, (b) degradation of MO with catalyst in dark, (c) under blue light photodegradation of MO, (d) under sunlight photodegradation of MO.

2. **Effect of degradation on variation of MO and TF-CD concentration**

Further, we performed a kinetics study for the varying concentrations of dye (5, 10, 15, 20, 25, and 30 ppm) for MO dye degradation using a TF-CDs catalyst under sunlight illumination. The degradation process is shown by the plot of C/C_0 versus time. Figure S11a shows the degradation of 5−30 ppm of MO dye within a time frame of 60 min. It demonstrates that 5, 10 and 15 ppm concentrations of dye were degraded to an extent of ~97.5 %, 96.8 % and 92.8 %, respectively) within 60 mins, whereas the higher concentration of MO dye (20, 25 and 30 ppm) degraded only 69.4 %, 52.7 % and 48.1 %, respectively within a time frame of 60 min. A control set of 10 ppm dye solution shows no degradation in the time frame of ~60 min. The photodegradation process follows the pseudo-first-order kinetic model according to the Langmuir−Hinshelwood method as discussed in main manuscript (MS). The kinetics plot is shown in Figure S11b as $\ln(C_0/C)$ versus time. Figure S11c indicates that as we increase the concentration of the catalyst the degradation of MO also increases which follows the pseudo-first-order kinetic model. The kinetic plot is shown in Figure S11d as $\ln(C_0/C)$ versus time.

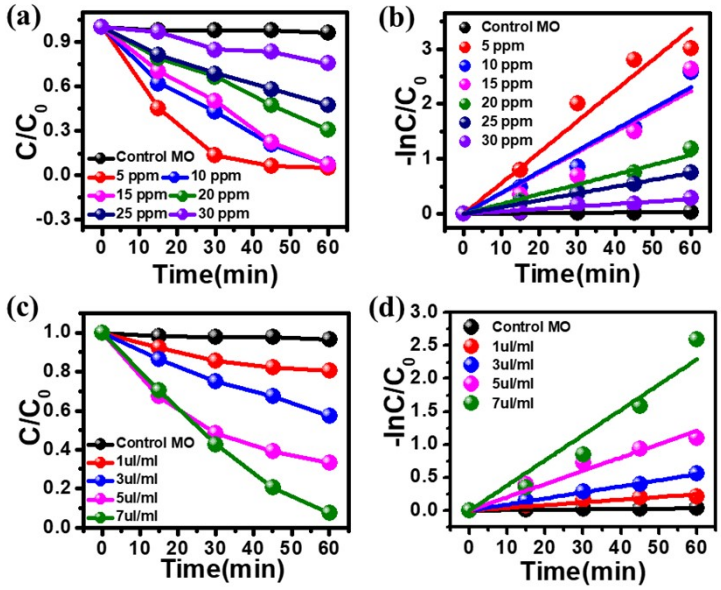

Figure S11. (a, b) Effect on photocatalyst on different concentration of MO and their rate, respectively and (c, d) Effect of different concentration of photocatalyst on MO and their rate, respectively.

3. **Effect of pH**

In Figure S12a the degradation rate was checked under different pH conditions and was found that at pH 2, the rate of degradation efficiency is maximum. Hence, all the experiments mentioned was carried out at pH 2. This is because of the surficial groups present on the catalyst and MO (having a sulfonate group and N═N bond molecules.[1] At neutral pH, catalyst has a negative zeta potential value (-8.43 mV). In acidic pH, the zeta potential values become positive (13.29 mV) due to the reduction in the negative charge on TF-CD and a fast electrostatic interaction was observed between positively charged TF-CD and anionic MO molecule. These are the favourable interactions occurred in the initial steps of the photodegradation phenomena. Also, the colour of MO changes from orange to red with a decrease in pH.[2] The generation of ROS takes place via absorption of photon under sunlight after the interaction of TF-CD and MO and degraded the MO molecule into lower hydrocarbons. In basic pH, TF-CD surface becomes more negatively charged (-26.66 mV) and a low degradation rate was observed due to hampered interaction with MO molecules.

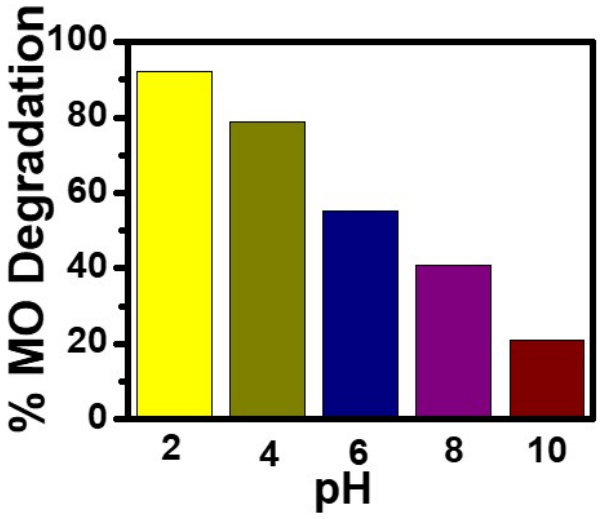

Figure S12. pH effect on MO degradation

Table S1. Comparison of photocatalytic performance towards MO by various types of photocatalysts**.**

Sr. No.	Catalysts	MO	Time (mins)	Degradation efficiency (%)	Light intensity	References
1	P-, S-codoped g-C_3N_4	1.0 g/L and 0.5 g/L	60	73.25	Visible light ($\lambda \geq$ 420 nm, 300 W xenon lamp	[3]
2	MIL-100 (Fe)-RT	5 ppm	480	64	150 W UV lamp	[4]
3	KAPs-B/Cu_2O	30 mg/L	60	92	visible light (500 W xenon lamp)	[5]
4	WO_3-TiO_2	0.06 mM	300	99	UV lamps T-15 L (15 W, λ_{max} = 365 nm	[6]
5	Co–ZnO	100 mg/L	130	93	visible light	[7]
6	ZnO-Al_2O_3-CeO_2-Ce_2O_3	20	300	99.8	250 W mercury lamp	[8]
7	MoS_2 nanoflower–TiO_2	20 mg/dm^3	80	93	UV–Visible Light (365 nm)	[9]
8	CQDs/TiO_2	40 ppm	360	78.75	365 nm ultraviolet light	[10]
9	PE-TiO_2 nanoparticles	0.1 mM	120	95	24 W light-emitting diode (LED) lamp	[11]
10	TF-CD	10 ppm	60	96.8	Under sunlight	This work

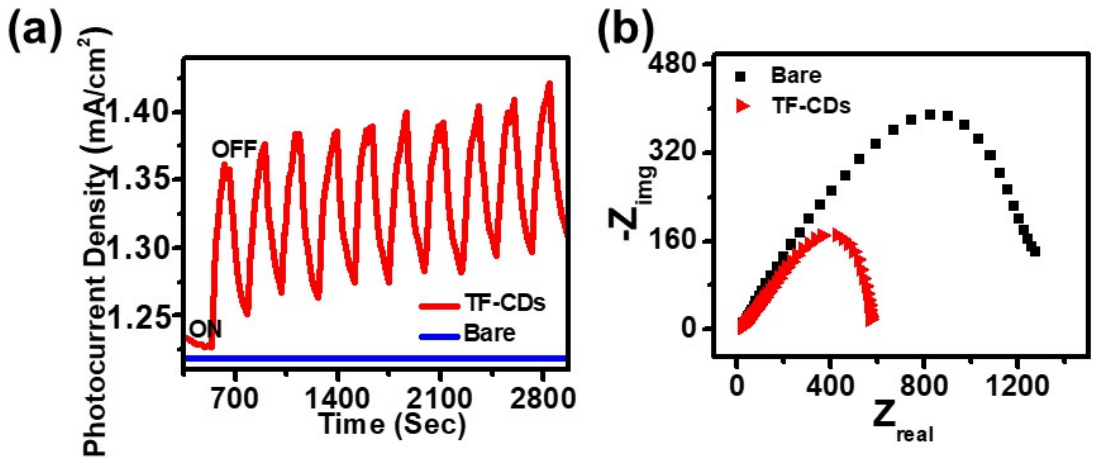

Figure S13. (a) Transient photocurrent density versus time plotted and (b) EIS Nyquist plots of TF-CDs under visible light in 0.5 M Na_2SO_4 electrolyte.

4. Degradation under sunlight in real water samples

The same photodegradation studies were performed to multiple water sources, including ground water (Simrol, Madhya Pradesh), tap water (corporation water, Simrol, Madhya Pradesh), and river water (Narmada River, Omkareshwari Temple, Madhya Pradesh). MO dye was spiked to these water sample. These spiked samples were then subjected to TF-CDs treatment (674 mg/mL; of 7 µL) under sunlight as described in the Experimental Section. The UV absorbance spectra of the initial and final spiked samples were taken. Table S2 displays the initial and final concentrations of water samples after degradation in sunlight that has contaminated with MO. Their UV analysis clearly indicates that MO in the spiked samples extensively degraded with an efficiency >95% in 60 min.

Table S2. Photodegradation of MO: initial and final dye concentration of MO spiked water samples containing TF-CD under sunlight irradiation.

Sr. No.	Spiked real sample	Initial concentration of MO dye (ppm)	Final concentration of MO dye (ppm)
1.	Ground water	10	0.04
2.	Tap water	10	0.06
3.	River water	10	0.05

References

1 Y. Sha, I. Mathew, Q. Cui, M. Clay, F. Gao, X. J. Zhang and Z. Gu, *Chemosphere*, 2016, **144**, 1530–1535.
2 M. S. Osgouei, M. Khatamian and H. Kakili, *Materials Chemistry and Physics*, 2020, **239**, 122108.
3 L. Jiang, X. Yuan, G. Zeng, X. Chen, Z. Wu, J. Liang, J. Zhang, H. Wang and H. Wang, *ACS Sustainable Chem. Eng.*, 2017, **5**, 5831–5841.
4 K. Guesh, C. A. D. Caiuby, Á. Mayoral, M. Díaz-García, I. Díaz and M. Sanchez-Sanchez, *Crystal Growth & Design*, 2017, **17**, 1806–1813.
5 Q. Zhao, K. Wang, J. Wang, Y. Guo, A. Yoshida, A. Abudula and G. Guan, *ACS Appl. Nano Mater.*, 2019, **2**, 2706–2712.
6 J. A. Pinedo-Escobar, J. Fan, E. Moctezuma, C. Gomez-Solís, C. J. Carrillo Martinez and E. Gracia-Espino, *ACS Omega*, 2021, **6**, 11840–11848.
7 M. Adeel, M. Saeed, I. Khan, M. Muneer and N. Akram, *ACS Omega*, 2021, **6**, 1426–1435.
8 F. Z. Janani, H. Khiar, N. Taoufik, A. Elhalil, M. Sadiq, A. V. Puga, S. Mansouri and N. Barka, *Materials Today Chemistry*, 2021, **21**, 100495.
9 S. V. Kite, A. N. Kadam, D. J. Sathe, S. Patil, S. S. Mali, C. K. Hong, S. Lee and K. M. Garadkar, *ACS Omega*, 2021, **6**, 17071–17085.
10 Y. Deng, M. Chen, G. Chen, W. Zou, Y. Zhao, H. Zhang and Q. Zhao, *ACS Omega*, 2021, **6**, 4247–4254.
11 K. Al-hamoud, M. R. Shaik, M. Khan, H. Z. Alkhathlan, S. F. Adil, M. Kuniyil, M. E. Assal, A. Al-Warthan, M. R. H. Siddiqui, M. N. Tahir, S. T. Khan, A. A. Mousa and M. Khan, *ACS Omega*, 2022, **7**, 4812–4820.